Chemical Physics 149 (1990) 63–80
North-Holland

Fundamental aspects of chemical kinetics in condensed phases

Jonathan G. Harris and Frank H. Stillinger
AT&T Bell Laboratories, Murray Hill, NJ 07974, USA

Received 16 May 1990

Solvents can exert strong effects on chemical reaction rates. The interaction of solvent with reactant species causes shifts in transition states, replacing the gas phase saddle point with a distribution of saddle points differing in height, extent of asymmetry, curvatures, etc. The effect of such a distribution on measured reaction rates can be assessed with an extension of the Stillinger–Weber inherent structure theory. This theory uses a mass-weighted descent mapping to partition the multidimensional configuration space into distinct potential energy "basins"; in the present work these are classified by the numbers of reactant and product species present at the minima. Chemical transition states are flanked by pairs of "gateway" basins. We have implemented this formalism numerically and located the actual chemical transition states for a molecular dynamics model of the exchange reaction $F+F_2 \rightleftharpoons F_2+F$ in liquid argon. In the dense solution, the frequency of trajectory recrossings through the transition state exceeds that in the gas phase reaction. Most of this difference stems from the changes in geometry of reactants at the distribution of reactive saddle points.

1. Introduction

The presence of solvent often exerts a profound influence on the attainable products of chemical reactions, and on the rates at which those products are created. The theory of chemical kinetics historically offers numerous and diverse attempts to explain solvent effects; perhaps the most notable are the Kramers theory [1], and the Eyring "absolute rate theory" adapted to solutions [2]. The scientific literature abounds in extensions and reinterpretations of these approaches [3]. More recently, equilibrium autocorrelation function expressions for reaction rates have been adduced [4–6], analogous to the Mori–Kubo–Zwanzig formulas for linear transport coefficients [7]. In addition, computer simulation studies of selected chemically reactive systems have begun to play an important conceptual role in this field [8–10].

The primary objective of the present study has been to examine chemical reactions in solvents at the most basic molecular level. The inherent structure theory of condensed phases supplies the necessary conceptual framework [11–14], and guides the formulation of a modernized "absolute rate theory". To give concrete meaning to our approach we report specific results for a computer study of the exchange reaction

$$F+F_2 \rightleftharpoons F_2+F \tag{1.1}$$

in liquid argon. While this is molecularly a simple case, it serves nevertheless to illustrate important general principles expected to apply to all condensed phase chemical reactions.

Section 2 introduces the inherent structure formalism as it applies to chemically reactive systems. Section 3 presents details of the fluorine–argon model, and section 4 outlines the various numerical simulation and analysis procedures employed in its study. Section 5 contains a collection of quantitative results obtained for the model. Section 6 illustrates the application of the inherent structure theory to the system. The concluding section 7 discusses implications of the present study for the general kinetic theory of reaction rates in solvents, and indicates principal useful directions for future work.

2. Inherent structures in reacting systems

In order to keep the following discussion as clear and straightforward as possible, we shall suppose that the system of interest consists of N_S inert solvent

molecules in which the following generic reversible chemical reactions occur:

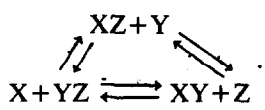

(2.1)

We assume that the numbers of distinct chemical species $N_X(t)$, $N_Y(t)$, $N_Z(t)$, $N_{XY}(t)$, $N_{XZ}(t)$, and $N_{YZ}(t)$ can be uniquely determined from the system dynamics at any time t.

A further assumption will be invoked, namely that the chemically reacting system remains on its Born–Oppenheimer ground-electronic-state energy hypersurface. Generalization of the following to include excited-state surfaces and associated transitions is certainly possible [15] but entails technical complications that are not germane to our specific application in section 3 et seq.

Let $\Phi(\boldsymbol{R})$ represent the potential energy function for the chemically reacting system. Here $\boldsymbol{R}$ comprises all configurational coordinates needed to specify the positions of solvent, reactant, and product particles; in the event that constant pressure conditions are used (rather than constant volume) $\boldsymbol{R}$ will also include volume V as a coordinate [16].

The central strategy of the inherent structure approach is to relate the instantaneous system configuration $\boldsymbol{R}(t)$ to that of a nearby relative potential energy minimum, say $\boldsymbol{R}_\alpha$. For this purpose it has been natural to employ the mapping to minima induced by solutions to the mass-weighted descent equations [16]:

$$\mathbf{m}\cdot d\boldsymbol{R}/du = -\nabla\Phi(\boldsymbol{R}). \tag{2.2}$$

Here $\mathbf{m}$ is the mass tensor and u is a virtual time parameter. Except for initial conditions with measure zero, the solutions to eq. (2.2) converge onto local minima of Φ as $u\to+\infty$. The collection of all $\boldsymbol{R}$s that map onto the $\boldsymbol{R}_\alpha$ for a given local Φ minimum defines the potential energy "basin" B_α. The collection of all $\boldsymbol{R}_\alpha$s for a given system comprises its "inherent structures". The mapping of the continuous dynamical configuration $\boldsymbol{R}(t)$ onto the piecewise constant inherent structure configurations $\boldsymbol{R}_{\alpha(t)}$ constitutes a natural coarse-graining of the system dynamics.

Prior simulation studies of chemically reactive systems [17,18] indicate that identification of chemical species is especially simple at the inherent structure configurations. We shall therefore take the point of view that the species numbers N_X, ..., N_{YZ} applicable for the configuration $\boldsymbol{R}_\alpha$ are the same throughout the entire basin B_α. In other words, intrabasin displacements are never regarded as producing a change in the numbers of chemical species.

The number of distinct inherent structures (potential energy minima) is expected to rise exponentially with N, the number of particles in the system, in the large system limit [11]. Consequently the collection of distinct inherent structures for a macroscopic system where N is of order Avogadro's number is indeed enormous. This situation permits a formal simplification in the description of thermal equilibrium because the potential energy minima and their basins can be classified by a small number of intensive order parameters, and measurable properties expressed in terms of distributions of basins over these order parameters.

At the simplest level of description one can utilize a single relevant order parameter, a convenient choice of which is the basin depth on a per-particle basis:

$$\phi = \Phi(\boldsymbol{R}_\alpha)/N. \tag{2.3}$$

In concordance with a preceding remark, the distribution of distinct basins with respect to ϕ is expected to have the form

$$\exp[N\sigma(\phi)], \quad \sigma(\phi)\geqslant 0, \tag{2.4}$$

where σ is N-independent in the large-N limit, with a form that depends on the specific solvent present. It is then straightforward to show that the free energy of the system is given by [11–14]

$$\beta F = \beta F_0 + \min_{(\phi)} [\beta f_v(\phi,\beta) + \beta\phi - \sigma(\phi)],$$

$$\beta = 1/k_B T, \tag{2.5}$$

where F_0 collects contributions to the free energy not stemming from interparticle interactions. The mean vibrational free energy per particle, for those basins with depth $N\phi$, has been denoted by f_v. The variational minimum in eq. (2.5) locates the depth of those basins which dominate at the prevailing temperature.

In the case of slowly relaxing degrees of freedom, eq. (2.5) can be extended to describe the resulting quasistatic regime. This demands that a larger set of descriptive order parameters be introduced [16]. If

the slow degrees of freedom are only those associated with the chemical relaxations in the reaction set (2.1), one can employ the four intensive order parameters

$$\xi=(\phi, C_X, C_Y, C_Z), \tag{2.6}$$

where $C_X=N_X/V$, etc. The distribution of basins in the extended order parameter space becomes

$$\exp[N\sigma(\xi)], \tag{2.7}$$

and eq. (2.5) becomes replaced by

$$\beta F=\beta F_0+\min_{(\xi)}[\beta f_v(\xi,\beta)+\beta\phi-\sigma(\xi)]. \tag{2.8}$$

This yields the equilibrium free energy in agreement with the corresponding result from eq. (2.5), but in addition the values of C_X, C_Y, and C_Z at the minimum give the equilibrium constants for the reacting systems. By carrying out a constrained minimization only over ϕ,

$$\beta F(C_X, C_Y, C_Z) = \beta F_0+\min_{(\phi)}[\beta f_v(\xi,\beta)+\beta\phi-\sigma(\xi)], \tag{2.9}$$

the resulting free energy at fixed chemical composition (i.e. "frozen" reactions) gives the thermodynamic driving force for chemical relaxation.

Fundamental system transitions between contiguous basins in the multidimensional configuration space occur as $\boldsymbol{R}(t)$ crosses a shared basin boundary. These transitions have been found to correspond to localized rearrangements of a small subset of particles in three dimensions [19,20]. At low temperature the $\boldsymbol{R}(t)$ crossing point is expected to occur close to a simple saddle point (transition state) embedded in the shared basin boundary.

If the chemically reactive species form a dilute solution in the inert solvent, the majority of the interbasin transitions will merely produce physical rearrangements of the solvent, but will not involve chemical change. However some of the interbasin transitions correspond to shifts in the pattern of covalent bonds, i.e. to chemical reaction.

Fig. 1 provides a schematic diagram of a portion of the basins in configuration space, particularly those neighboring an extended surface across which the lowest reaction in (2.1) changes the affected species numbers by ± 1. Obviously each transition state (saddle point) in this extended boundary is flanked

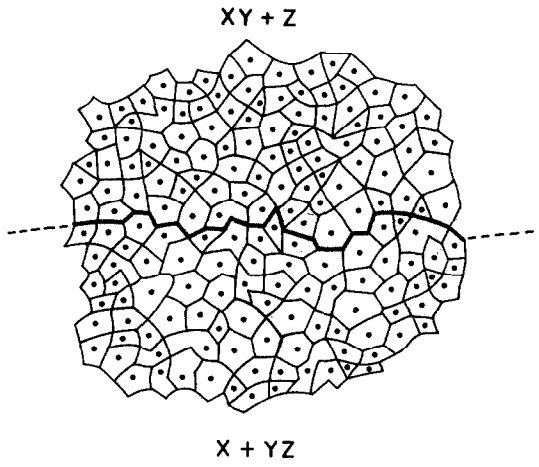

Fig. 1. Schematic diagram of a portion of the multidimensional configuration space showing minima, basins, and an extended surface across which reaction occurs. Chemically relevant transition states occur in this extended surface, and are flanked by pairs of "gateway" basins. Each basin contains a single local minimum of the potential energy, with a position denoted by a dot.

by a pair of "gateway" basins. The transition states and flanking basins will vary in their properties, such as barrier height, curvatures, anharmonicities, recrossing probabilities, etc. The chemical reaction rates clearly depend upon the distributions of these characteristics, which are induced by the presence of the solvent. A proper and complete theory of solvation effects on reaction rates must account for these distributions in a detailed way. Contributing to this objective is the goal of the specific simulation reported in the following sections.

The inherent structure formalism suggests a natural form for rate constants. We will compare this form to the "variational" theory of reactions in solution for an atom–diatom exchange,

$$XZ+Y\rightleftharpoons X+ZY, \tag{2.10}$$

in a dilute solution. In the following discussion, the chemical species on the left-hand side are the reactants, those on the right side the products. The generalization of this discussion to high reactant concentrations is straightforward.

The variational transition state theory rate constant is

$$k_v = \frac{k_B T}{Q_R h P} \int_{\Omega} \exp[-\beta\Phi(R)]\, dR^{3N-1}, \qquad (2.11)$$

where Q_R is the reactant partition function in a system with $3N$ degrees of freedom, P is the number of particle permutations which produce indistinguishable configurations, and Ω is a $(3N-1)$-dimensional dividing surface which separates the two distinct chemical states [21]. This expression is an upper bound on the true rate constant since some of the flux across the surface does not contribute to the net creation of product – e.g., trajectories which cross the dividing surface and turn back within a time much shorter than the average lifetime of the products. The ratio of the total flux across the dividing surface to the reaction flux defines the recrossing correction, $0 \leqslant \kappa \leqslant 1$. In the rigorous canonical variational treatment, Ω is the surface minimizing k_v [21]. In the condensed phase, identifying this surface is frequently impractical, thus the choice of dividing surfaces is limited to a family which can be specified by constraining one degree of freedom, Δ (usually the gas phase reaction coordinate). The integral in eq. (2.11) is $\exp[-F(\Delta)/k_B T]$, where the function $F(\Delta)$ is the potential of mean force (aside from an additive constant). The reaction rate is then computed at the value of Δ maximizing $F(\Delta)$ [22]. We will refer to the surface defined by constraining Δ to the value maximizing the potential of mean force as the "variational transition surface", although this surface certainly differs from the best multidimensional variational surface.

Within the inherent structure formalism, a transition state rate constant can be defined as

$$k_I = \frac{k_B T}{h} \frac{1}{Q_R} \sum Q(\boldsymbol{S}_\alpha) \exp[-\beta\Phi(\boldsymbol{S}_\alpha)], \qquad (2.12)$$

where the sum is taken over saddle points $\boldsymbol{S}_\alpha$ separating reactant basins from product basins ("reactive saddle points"),

$$Q(\boldsymbol{S}_\alpha) = \frac{1}{h^{3N-1} P} \times \int_{\Omega_\alpha} \exp\{-\beta[\Phi(\boldsymbol{R}) - \Phi(\boldsymbol{S}_\alpha)]\}\, d\boldsymbol{R}^{3N-1}, \qquad (2.13)$$

with P the permutation factor. The dividing surfaces Ω_α are the loci of points which are mapped onto $\boldsymbol{S}_\alpha$ by the descent equation, eq. (2.2). These points form a $(3N-1)$-dimensional surface embedded in the full $3N$-dimensional space and are part of the set of measure zero which is not mapped into a local minimum by the descent equations. The collection of these surfaces is the "inherent structure transition surface". Points infinitesimally displaced from these dividing surfaces in opposite directions are mapped by the descent equations into gateway minima corresponding to different chemical species. The weight of each saddle point in eq. (2.12) is proportional to the factor $Q(\boldsymbol{S}_\alpha) \exp[-\beta\Phi(\boldsymbol{S}_\alpha)]$. Finally, eq. (2.12) does not account for recrossings of the inherent structure dividing surface.

3. Potential energy surface

Our model system consists of three fluorine atoms in argon. The potential energy surface can be broken up as

$$\Phi(\boldsymbol{R}) = \Phi_{F\text{-}F}(\boldsymbol{R}_F) + \Phi_{Ar\text{-}Ar}(\boldsymbol{R}_{Ar}) + \Phi_{Ar\text{-}F}(\boldsymbol{R}), \qquad (3.1)$$

where the various respective contributions are from the fluorine–fluorine, argon–argon, and fluorine–argon interactions. The interactions are selected to achieve reasonable agreement with available experimental data. We also require all derivatives of the potential to be continuous for all real coordinates away from atomic superposition and to vanish beyond fixed positive interparticle separations.

For clarity in the rest of this work we treat the fluorine atoms as distinguishable particles and examine only the exchange reaction in eq. (2.10) where X, Y, and Z correspond to atoms 1, 2, and 3. The interaction between the fluorine atoms (fig. 2) is that originally proposed by Stillinger and Weber [18], with a slight change in the parameters. It can be broken up into two body (u_2) and three body (u_3) functions of the positions, $\boldsymbol{r}_i$, of the individual fluorine atoms,

$$\Phi_{F\text{-}F}(\boldsymbol{R}_F) = \sum_{i<j} u_2(\boldsymbol{r}_i, \boldsymbol{r}_j) + \sum_{i<j<k} u_3(\boldsymbol{r}_i, \boldsymbol{r}_j, \boldsymbol{r}_k). \qquad (3.2)$$

The pair potential is

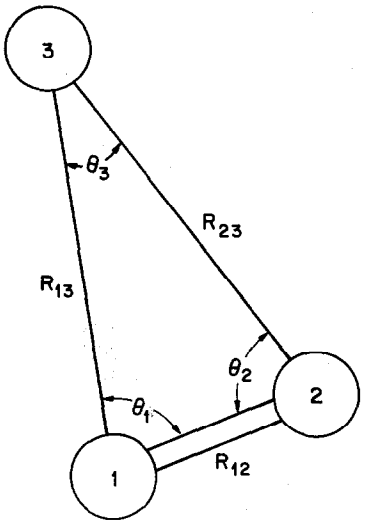

Fig. 2. The isosceles triangle minimum energy arrangement of three fluorines shown with the variables used in potential energy function formulas.

$$u_2(r)=A_1\epsilon_{F\text{-}F}\left[\left(\frac{r}{\sigma_{F\text{-}F}}\right)^{-8}-\left(\frac{r}{\sigma_{F\text{-}F}}\right)^{-4}\right]$$
$$\times\exp\left[\left(\frac{r}{\sigma_{F\text{-}F}}-rc_{F\text{-}F}\right)^{-1}\right], \qquad (3.3)$$

where r is the interatomic distance, $\sigma_{F\text{-}F}=1.2141$ Å, $A_1=6.052463017$, defined so that well depth is $\epsilon_{F\text{-}F}$ (160.2263 kJ/mol), $rc_{F\text{-}F}=3.6$, and the interaction vanishes when $r>rc_{F\text{-}F}\sigma_{F\text{-}F}$. By construction this potential produces a bound diatomic molecule with a dissociation energy of 160.2263 kJ/mol, a bond length of 1.435 Å, and a vibrational frequency of 896.9 cm^{-1}. These properties are all very close to the experimentally determined values for the F_2 molecule [23,24].

The three body potential, which is required to ensure that the lowest energy configuration consists of bound diatomic molecules, is

$$u_3(\boldsymbol{r}_1,\boldsymbol{r}_2,\boldsymbol{r}_3)=\nu(r_{12},r_{13},\theta_1)+\nu(r_{23},r_{13},\theta_3)$$
$$+\nu(r_{12},r_{23},\theta_2), \qquad (3.4)$$

where,

$$\nu(r,s,\theta)=\nu_1(r/(\sigma_{F\text{-}F}),s/(\sigma_{F\text{-}F}))$$
$$+\nu_2(r/(\sigma_{F\text{-}F}),s/(\sigma_{F\text{-}F}),\theta). \qquad (3.5)$$

The functions ν_1 and ν_2 of the bond angle and scaled distances are

$$\nu_1(r,s)=c_1(rs)^{-4}\exp[(r-c_2)^{-1}+(s-c_2)^{-1}] \qquad (3.6)$$

when $0<r<c_2$ and $0<s<c_2$, and

$$\nu_2(r,s,\theta)=(c_3-c_4\cos^2\theta)$$
$$\times\exp[c_5(r-c_6)^{-1}+c_5(s-c_6)^{-1}], \qquad (3.7)$$

when $0<r<c_6$ and $0<s<c_6$, and where the parameters c_1 through c_6 are respectively 1345.9 kJ/mol, 3.6, 8812.44 kJ/mol, 4005.657 kJ/mol, 3.0, and 2.8. The parameter c_3 is 1.1 times greater than the original Stillinger–Weber potential in order to guarantee that at the transition state, the molecule is linear, the two bond lengths are equal, and there is a negative curvature along the asymmetric stretch coordinate [18]. c_2 and c_6 define cutoff radii. When r or s exceeds c_2, ν_1 vanishes, and when either exceeds c_6, ν_2 vanishes.

Three isolated fluorine atoms will have two distinct local minima, a linear geometry (F–F distances 1.443 and 2.832 Å, and energy −166.47 kJ/mol), and an isosceles triangle (one F–F distance of 1.449 Å, and the other two 2.909 Å, energy −171.45 kJ/mol). The transition state (saddle point of the energy) is linear with an energy of −137.79 kJ/mol and two equal F–F distances of 1.657 Å. The reaction path, consisting of the two trajectories from the transition state, goes directly to the two flanking linear local minima. We should point out that as of the time of this writing the geometry of the real fluorine transition state has not been determined either experimentally or by ab initio quantum mechanical calculations.

The gas phase reaction coordinate for the fluorine atom–diatom exchange reaction (eq. (1.1)) is the asymmetric stretch, $\Delta=R_{12}-R_{23}$. At the gas phase transition state $\Delta=0$, and the unit vector along the asymmetric stretch coordinate is an eigenvector of the Hessian matrix of second derivatives of the potential energy surface. The corresponding eigenvalue is -454.71 ps^{-2}.

The argon–argon interactions include only a pair potential of the form utilized by Stillinger and Weber [12],

$$u(r)=A_2\epsilon_{\mathrm{Ar-Ar}}\left[\left(\frac{r}{\sigma_{\mathrm{Ar-Ar}}}\right)^{-12}-\left(\frac{r}{\sigma_{\mathrm{Ar-Ar}}}\right)^{-5}\right]$$
$$\times\exp\left[\left(\frac{r}{\sigma_{\mathrm{Ar-Ar}}}-d_1\right)^{-1}\right], \tag{3.8}$$

where $A_2=6.767441$ so that the well depth is $\epsilon_{\mathrm{Ar-Ar}}=0.997615$ kJ/mol, $\sigma_{\mathrm{Ar-Ar}}=3.4$ Å, and the cutoff beyond which the pair interaction vanishes, d_1 is 2.46491832.

The argon–fluorine interaction is of the same form as eq. (3.8), but with $\sigma_{\mathrm{Ar-F}}=3.0904$ Å, $\epsilon=0.74992$ kJ/mol, and the same cutoff at 2.46491832. The application of the combining rules

$$\epsilon_{\mathrm{Ar-F}}=\tfrac{1}{2}(\epsilon_{\mathrm{Ar-Ar}}+\epsilon_{\mathrm{F-F}}) \tag{3.9}$$

and [25]

$$\sigma_{\mathrm{Ar-F}}=(\sigma_{\mathrm{F-F}}\sigma_{\mathrm{Ar-Ar}})^{1/2} \tag{3.10}$$

to the parameters used in our fluorine pair interaction would give an attraction which is far too strong and a core radius which is probably too small. The fluorine interaction parameters inserted in eqs. (3.9) and eqs. (3.10) to obtain our values are those used by Singer, Taylor, and Singer [26] to model liquid F_2 as rigid diatomic molecules consisting of two Lennard-Jones centers.

Our core radius of the Ar–F interaction is slightly larger than that used by Gerber and co-workers [10] in their simulation of the photodissociaton of F_2 in an argon lattice. Likely a realistic F–Ar potential would involve three body F–F–Ar interactions which would interpolate between the extremes of the bare F–Ar interaction and the F–Ar interaction of the F_2 molecule. The effects of leaving out this effect will be discussed later in the paper.

4. Methods

In this section we describe the methods used in carrying out molecular dynamics simulations, obtaining the saddle points, and locating minima. Molecular dynamics simulations are used to (1) compute free energies of activation in the variational transition state theory using the thermodynamic integration method [27,28], (2) study the Ar–F pair correlation functions of the transition state complex, and (3) generate trajectories through the variational transition state surface in order to locate saddle points and to analyze the crossings of this surface.

The Newtonian equations of motion are integrated using the velocity Verlet algorithm [29] with a time step of 0.001 ps when generating trajectories through the variational transition surface, and 0.003 ps in all other calculations. To perform some of the calculations such as the free energy integration required to determine the potential of mean force as a function of the fluorine asymmetric stretch, it is necessary to hold constant the value of the asymmetric stretch. In these cases Andersen's algorithm, RATTLE, is used to solve the constrained Lagrangian equations of motion [29]. We omit the corrections for the Jacobian due to the usage of constraints [30,31]; because bond length constraints have only small effects on equilibrium properties computed from the simulation of organic molecules, it is likely that this correction is small in the present work especially around the transition states where the fluorines are almost linear [31,32]. Berendsen's algorithm [33] with relaxation times between 0.2 and 0.5 ps is used to maintain a constant temperature of 150 K, except when generating reactive trajectories, in which case only Newtonian dynamics (microcanonical) was used. Simulations start by randomly placing the argons in an $18\times18\times18$ Å box. The three fluorine atoms must be held fixed at the gas phase transition state until the potential energy approaches its equilibrium value; otherwise the strong forces present in the initial configuration could rip the fluorines apart. Periodic boundary conditions were maintained in all three directions. Three argon densities of 0.73 (64 Ar atoms), 1.42 (125 Ar atoms), 1.71 g/ml (150 Ar atoms) were studied.

In the last case, the argon freezes to a hexagonal close packed structure with the three fluorines replacing two argon atoms. This may be a metastable structure, since at zero temperature and pressure the minimum energy configuration with our pair potential is the face centered cubic crystal [34]. It is also possible that the periodic boundary conditions inhibit the formation of the face centered cubic crystal in this fairly small system.

Potentials of mean force as a function of the asymmetric stretch are computed using the free energy integration algorithm [27]. The difference between the potentials of mean force at Δ_1 and at Δ_2 is

$$F(\Delta_2)-F(\Delta_1)=\int_{\Delta_1}^{\Delta_2}\langle \mathrm{d}\Phi/\mathrm{d}\Delta\rangle_\Delta \,\mathrm{d}\Delta. \tag{4.1}$$

$\langle\ \rangle_\Delta$ refers to an average over an ensemble with the asymmetric stretch of the fluorines constrained to a value Δ. The integration is carried out from $\Delta=-2.0$ Å to $\Delta=+2.0$ Å in N_{step} time steps, incrementing Δ by $\delta\Delta_t=(\Delta_2-\Delta_1)/(N_{\text{step}}-1)$ at each time step. In the solution phase, 1 million time steps are used. When the isolated fluorine complex was studied, we used 20 million time steps with velocities randomized every other time step to sample the configuration space thoroughly. The potential of mean force is computed from the discretized version of eq. (4.1),

$$F(\Delta_2)-F(\Delta_1)=\sum_{t=t_1}^{t_2}\frac{\mathrm{d}\Phi(\boldsymbol{R}_t)}{\mathrm{d}\Delta}\delta\Delta_t. \tag{4.2}$$

Because the constraint is varied at a finite rate, there are slight errors from the failure of the system to remain at equilibrium at all times. This error shows up in the failure of the computed potential of mean force to reflect the reaction's symmetry about $\Delta=0$. In the examples reported here, this free energy difference between $\Delta=+2.0$ and $\Delta=-2.0$ Å is about 1.0–1.6 kJ/mol with 125 argons (1 million time steps of 0.003 ps) and 0.05–0.1 (20 million 0.003 ps time steps) for the isolated fluorines. When the results of both halves of the reaction ($\Delta<0$ and $\Delta>0$) are averaged, this error, as well as the uncertainty from the statistical sampling, is substantially reduced. Although the expense of the potential of mean force calculations (4 Cray hours for a 1 million step run on the system with 125 argons) makes the computation of more than a few potential of mean force curves for a given set of physical conditions impractical, the variation of the free energy of activation with the size of the time step and the length of the run show that errors from these limitations are much smaller than the effects discussed in this work. The results for the 125 argon system are verified by a simulation of 2 million 0.003 ps time steps which predicts a free energy difference between $\Delta=-2.0$ and $\Delta=+2.0$ Å of only 0.1 kJ/mol.

In the fluorine trapped in the solid argon, the free energy integration was repeated twice after heating the sample at 1000 K for 30 ps and recrystallizing with a 2300 ps equilibration period at 150 K. The resulting free energy of activation in this group of simulations is 0.5 kJ/mol lower than that from the original ones reported in section 5. Given the long relaxation times of the solid, this should not be surprising.

To locate saddle points and examine crossings of the transition surfaces, we use configurations sampled 6.0 ps apart in a molecular dynamics simulation carried out with the asymmetric stretch constrained to zero. Trajectories are generated from each configuration by assigning velocities from the Boltzmann distribution at 150 K to all atoms and evolving the system to positive and negative times at constant total energy using the velocity Verlet algorithm with a time step of 0.001 ps. This procedure generates trajectories through the variational transition surface with probabilities proportional to their Boltzmann weights.

Crossings of the variational transition surface are identified by a change in sign of Δ along the trajectory. Crossings of the inherent structure transition surface are distinguished by a change in the sign of the Δ defined for each local minimum. Generally this involves a change from $\Delta\approx\pm1.4$ to $\Delta\approx\mp1.4$ Å. The sign of Δ can be determined usually by fewer than 1000 iterations of a descent calculation from the point along the trajectory.

The property of the inherent structure dividing surface in separating points mapped to different chemical species suggests a straightforward way of locating the saddle points. Two points along the trajectory on opposite sides of the dividing surface are identified. The basin of a point along the portion of the trajectory between them is identified used the descent calculation. The two points closest together but on opposite sides of the dividing surface are selected, and the procedure repeated until two points are arbitarily close together but on opposite sides of the dividing surface are located. A descent trajectory from these points should pass very close to the saddle point which can be identified by the nearly vanishing magnitude of the gradient and the existence of an imaginary frequency mode resembling the asymmetric stretch of the three fluorines.

Unfortunately, the hypothetical procedure outlined above would involve repeated expensive steepest descent calculations and would converge very slowly. Furthermore, as the starting points along the reaction trajectory get closer together more precise

(smaller "time step") descent calculations are required to identify the basin. We therefore have developed a three step procedure to locate the saddle points efficiently. Currently it is impossible to determine conclusively whether the saddle points located from a trajectory by our procedure are the appropriate ones for the trajectories as defined by the descent rule.

The first step of our algorithm uses the method of the previous paragraphs to obtain an initial approximation to the saddle point. Once a trajectory point close to the dividing surface is identified, a descent trajectory is run until the gradient starts increasing; this point along the descent path is the "initial guess' used by the next stage.

The rest of the computation is performed upon the mass-weighted coordinates,

$$x_i = (m_i)^{1/2} r_i, \tag{4.3}$$

where m_i is the mass of the ith atom (in amu). The second stage is an energy maximization along the approximate reaction coordinate and a steepest descent normal to it. The Hessian matrix of second derivatives of the potential energy is computed and diagonalized. The reaction coordinate – the mode having the greatest overlap with asymmetric stretch – is identified. Steepest descent calculations are carried out in the directions normal to this mode. At each iteration the position along the reaction coordinate is adjusted in the direction of increasing potential energy by the lesser of a maximum step length and the Newton–Raphson step that would make the gradient along the reaction path vanish (based on the gradient computed at the beginning of the step and the eigenvalue of the most recent Hessian). This procedure is typically carried out for about 10–20 thousand iterations with the Hessian recalculated at every thousand iterations.

In the third stage, the saddle point is located using the algorithm of Baker [35] modified to handle a large number of degrees of freedom. Along each mode, the magnitude of the step is the minimum of that determined by Baker's formulas and the maximum step size set by the user. Each iteration can be broken into two halves: (1) stepping in all directions normal to the reaction coordinate, and (2) stepping along the reaction coordinate. In the first half, the energy should decrease and in the second it should increase. Typically well over one thousand iterations are required to locate a saddle point in a system of 125 argon and 3 fluorine atoms. Direct application of this algorithm is encumbered by the time required to diagonalize the Hessian matrix; locating a saddle point in this region requires over 8 h of time on a Cray X/MP28. Hence the Hessian is recalculated and rediagonalized only when (1) the energy change since the Hessian was last computed is larger than a threshold (i.e. 3–12 kJ/mol), (2) the energy no longer decreases in the first half of the iteration, or (3) the number of iterations carried out since the last computation of the Hessian exceeds a threshold (usually 1000). The second half of the iteration is discarded if the energy does not decrease. Both halves of the first iteration with a new Hessian are always carried out. By reusing the Hessian, the time required to locate one saddle point in the 125 argon system is reduced to between 10 and 20 min on the Cray. Convergence is defined to have occurred when the norm of the gradient, the maximum magnitude of a component of the gradient along an eigenvector of the Hessian, the norm of the step size, and the maximum magnitude of a component of the step along an eigenvector of the Hessian have all become smaller than their respective upper bounds.

Actual reaction paths from a saddle point are found by perturbing the system in both directions along the mode with the negative eigenvalue and following the descent paths all the way to the two gateway minima. When only the gateway minima are desired, it suffices to start with a few thousand iterations of the descent with a time step of 0.00005 and then apply MINOP (which uses a dogleg strategy) to the mass weighted coordinates [36]. In cases where both the MINOP procedure and the full descent calculation were carried out until a minimum was located, the results were identical, except for one instance with a substantial energy difference.

5. Equilibrium properties of fluorine in argon

Figs. 3 and 4 show the Ar–F pair correlation functions for both an isolated fluorine atom and the F_3 complex within the variational transition surface, i.e. with the constraint $\Delta = 0$. These figures show the geometric screening of the middle fluorine atom by its

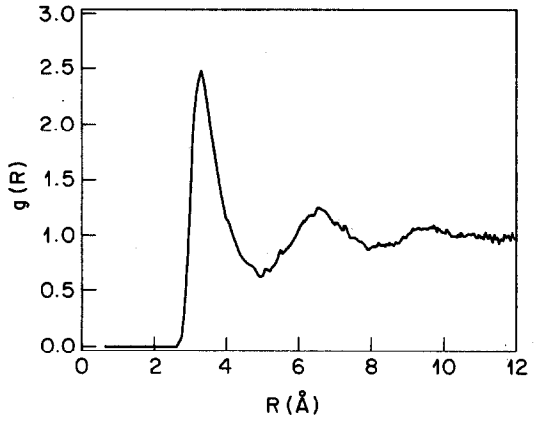

Fig. 3. The fluorine–argon pair correlation function at $T=150$ and $\rho_{Ar}=1.42$ g/ml (125 argon atoms) for an isolated F atom in argon.

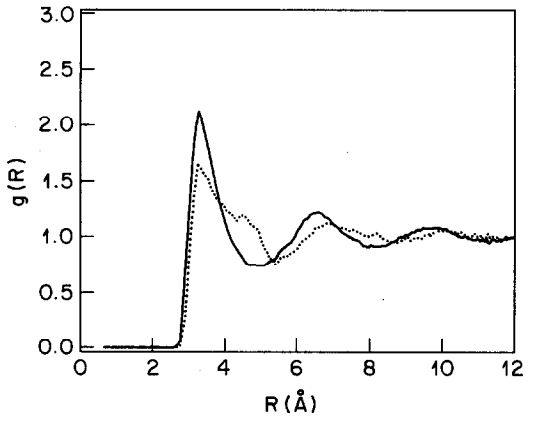

Fig. 4. The fluorine–argon pair correlation function at $T=150$ and $\rho_{Ar}=1.42$ g/ml (125 argon atoms) for the end (solid line) and central (dotted) atoms of the transition state F_3 complex in argon.

two neighbors as a broadened peak in its pair correlation function.

Fig. 5 illustrates the potential of mean force as a function of the gas phase reaction coordinate, the asymmetric stretch. In all cases the potential of mean force is maximized when $\Delta=0$. In the high density cases, the free energy of activation (the potential of mean force at $\Delta=0$ relative to $\Delta=\infty$) is decreased by solvation effects. In the solid we are likely studying a metastable system, and as mentioned earlier there

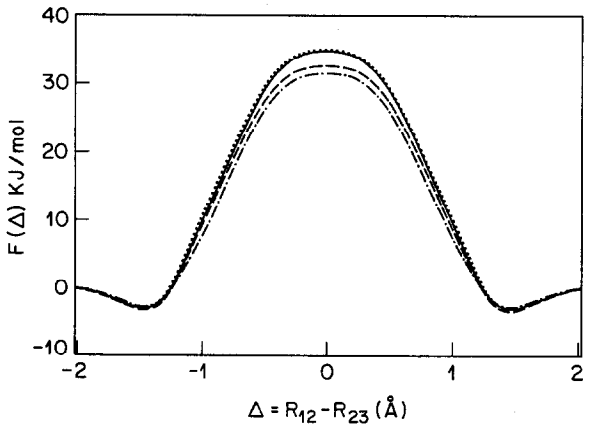

Fig. 5. The potential of mean force as a function of the asymmetric stretch for bare fluorine (solid line), and fluorine in argon at $T=150$ K and $\rho_{Ar}=0.73$ g/ml (dotted line), 1.42 g/ml (dashed), 1.71 g/ml (dot-dashed line). When $\rho_{Ar}=1.71$ g/ml, the argon has frozen into a hexagonal close packed lattice.

Table 1
Solvation effects on the transition state [a]

Ar density (g/ml)	Ar number	$\Delta F^{\ddagger}$ (kJ/mol)	k_R
0.00	0	34.8	1.0
0.73	64	34.9	0.9
1.42	125	32.7	5.3
1.71	150	31.9	10.2

[a] k_R is the ratio of the transition state rate constant to the gas phase value, $\Delta F^{\ddagger}$ is the free energy of activation measured relative to the free energy at $\Delta=2.0$ Å.

appears to be a slight shift in the potential of mean force curve following an annealing of the sample. It should also be recognized that any structural transitions responsible for this shift are much slower than the dynamics which determine the fate of the reactants.

The decrease in the free energy of activation appears to be due to an excluded volume effect. The "volume" of the transition state is slightly lower than that of the isolated fluorine atoms plus a bound diatomic molecule due to the geometric shielding of the inner fluorine by its two neighbors. The inner fluorine is also shielded from the attractive forces of the argon. At low density and temperature when packing is not a consideration, it is not unlikely that solvation effects would increase the activation free energy

slightly; however, the difference between the free energy of activation in 0.73 g/ml argon and the bare fluorine is within the uncertainty of the calculation. As shown in table 1, the change in the free energy of activation in our highest density liquid produces a five-fold increase in the variational reaction rate.

6. Inherent structures and reaction rates

The effect of the inherent structure on the reaction rate can be characterized by studying recrossings of our variational transition surface (defined by the condition $\Delta=0.0$).

Recrossings of this surface can result from two possible effects. In the first, which would be expected to dominate at high temperature, trajectories can be reflected across the dividing surface, even after crossing over a reactive saddle point, by features of the potential energy surface such as "bottlenecks" on the product side of the phase space [37]. Included in this class of recrossings are some caused by collisions between solvent and reactant molecules.

In the second case, which would dominate at low temperatures and strong solvation, the real saddle points are shifted from the $R_{12}=R_{23}$ hyperplane; consequently, trajectories which are close to a reaction path would not be near a saddle point when crossing the variational transition surface. As the system evolves towards the products, the potential energy must continue to increase as the saddle point is approached. If the velocity along the reaction coordinate is too small or the reaction coordinate is contorted, then the saddle point will not be reached and the solvation forces will pull the atoms back toward the reactant basin resulting in a recrossing of the variational transition surface. This picture is similar to that of the frozen adiabatic solvent model of Gertner et al. [38] which replaces the solvent with one "coordinate" that can shift the position of the transition state. This picture is most appropriate when the motion along the reaction coordinate is rapid enough so that the system either remains in the basins of attraction of one reaction path or at least with a family of reaction paths of similar saddle point structures and energies.

The relative importance of the two effects can be determined by comparing the number of crossings of the variational transition surface with the number of crossings of the inherent structure transition surface. Table 2 shows the number of crossings of the $\Delta=0$ surface and of the inherent structure transition states of 281 trajectories in the $\rho_{Ar}=1.42$ g/ml liquid and 201 reaction trajectories for the bare fluorine. Each trajectory was started from a different spatial configuration at the variational transition surface using the procedure outlined earlier. The role of the solvent can be identified by comparing the number of gas phase crossings to solution phase crossings. These statistics show that most of the cases with three or more crossings of the $\Delta=0$ plane can be attributed to characteristics of the gas phase potential energy surface; while most the incidences of two crossings (i.e. reactants back to reactants) are solvent induced. Table 2 also shows that in the gas phase at 150 K, the inherent structure dividing surface and the variational dividing surface are almost identical. Most importantly, well over half of the trajectories which cross the variational transition surface twice, never cross a saddle point. Furthermore, of the trajectories crossing the variational transition surface, the fraction crossing the inherent structure transition surface more than once is actually slightly larger in the gas phase (where the two surfaces are almost equal)! Unfortunately our present methods do not allow us to determine how many trajectories cross the inherent structure transition surfaces without crossing the variational transition surface.

Using the methods already described, we have located 185 reactive saddle points from 215 trajectories of the system with 125 argons ($\rho_{Ar}=1.42$ g/ml). The other 30 trajectories never crossed the inherent structure transition surface. We have also identified two reactive saddle points for fluorine trapped in the hexagonal close packed lattice.

When the reaction occurs in the liquid, the path between the reactive saddle point and the gateway minimum involves a significant rearrangement of the solvent molecules. Figs. 6–9 show two transition states and one gateway minimum of each transition state. In both of these cases the neighboring solvent molecules in the local minima have moved significantly from the original positions at the transition state. In contrast, when the reaction occurs in the solid, the arrangement of the solvent molecules is almost completely unchanged, as demonstrated by figs. 10 and

Table 2
The variational versus inherent structure transition surface: number of crossings at 150 K – fraction of trajectories through variational surface [a)]

Number of crossings	Isolated F_3		F_3 in Ar, $\rho_{Ar}=1.42$ g/ml	
	variational	inherent structure	variational	inherent structure
0	0	0	0	0.10
1	0.88	0.88	0.78	0.80
2	0.05	0.05	0.16	0.064
3	0.04	0.04	0.043	0.025
4	0.01	0.01	0.014	0.007
5	0.01	0.01	0.0041	0
6	0	0	0	0
7	0	0	0.004	0
8	0	0	0	0
9	0	0.01	0	0
10	0.01	0	0	0

[a)] Each entry is the fraction of trajectories started from the variational dividing surface which cross the corresponding dividing surface n_c times. The n_c are in the first column.

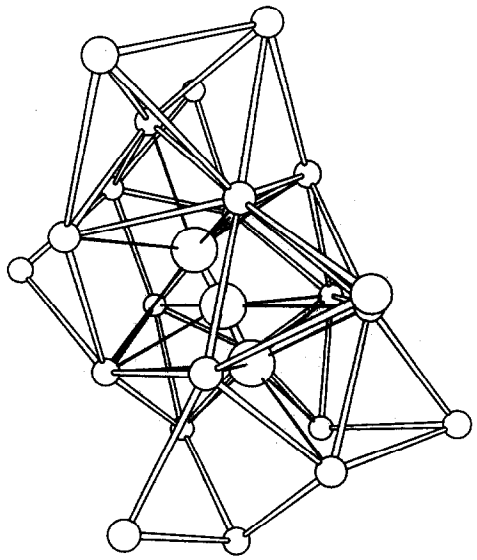

Fig. 6. A reactive saddle point of the fluorine in argon with $\rho_{Ar}=1.42$ g/ml, $T=150$ K. All argons within 6 Å of a fluorine atom are shown.

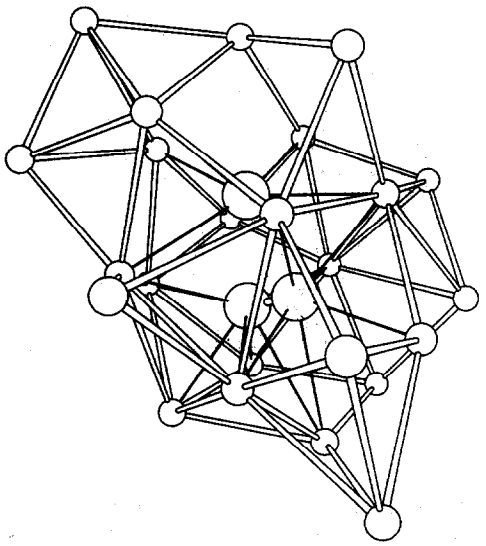

Fig. 7. A gateway minimum of the reactive saddle point of fig. 6 with $\rho_{Ar}=1.42$ g/ml, $T=150$ K. All argons within 6 Å of a fluorine atom are shown.

11 of a reactive transition state and its gateway minimum in solid argon.

This contrast between the reaction occurring in the liquid, solid, and gas phases is further illustrated by the features of the reaction paths shown in figs. 12–23. The properties are plotted as a function of the cumulative distance (in mass weighted coordinates) traveled along the reaction path,

$$d_{\text{path}} = \sum_{u=0}^{t} \delta_u \,, \tag{5.1}$$

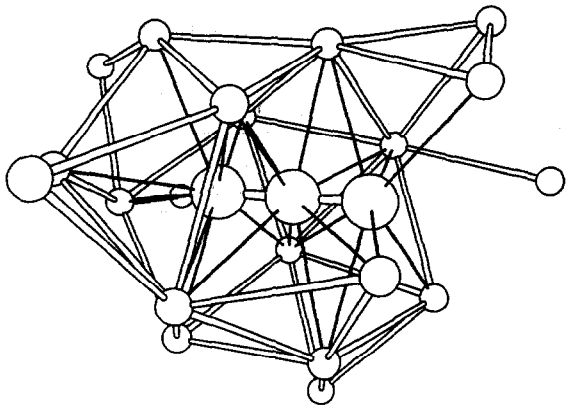

Fig. 8. Another reactive saddle point of the fluorine in argon with $\rho_{Ar}=1.42$ g/ml, $T=150$ K. All argons within 6 Å of a fluorine atom are shown.

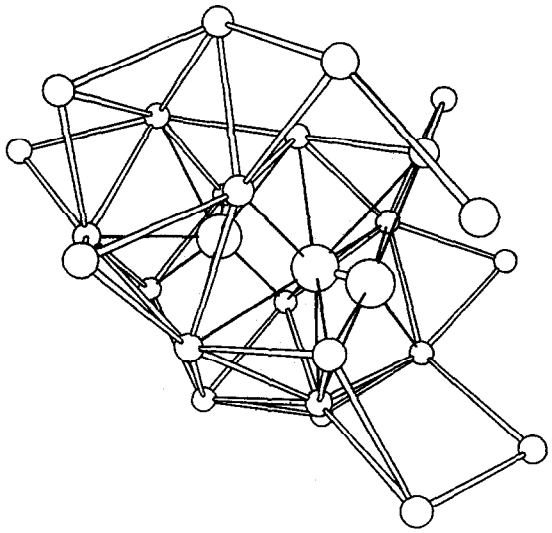

Fig. 9. A gateway minimum of the reactive saddle point of fig. 8 with $\rho_{Ar}=1.42$ g/ml, $T=150$ K. All argons within 6 Å of a fluorine atom are shown.

where

$$\delta_u = \left(\sum_{j=1}^{3N} [x_j(u+\mathrm{d}u) - x_j(u)]^2 \right)^{1/2} \qquad (5.2)$$

and $x_j(u)$ and $x_j(u+\mathrm{d}u)$ are the mass-weighted coordinates at virtual time u and $u+\mathrm{d}u$.

The figures show that in the dense liquid, the reaction path can be quite contorted and asymmetric around the saddle point, with the ratio of path length to the linear distance traveled from saddle point to a gateway minimum being approximately 2:1. This can

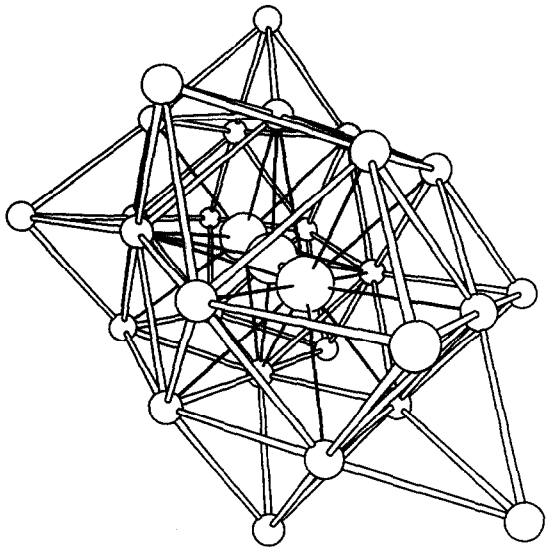

Fig. 10. A reactive saddle point of F_3 in hexagonal close packed argon at $\rho_{Ar}=1.71$ g/ml, $T=150$ K. All argons within 6 Å of a fluorine atom are shown.

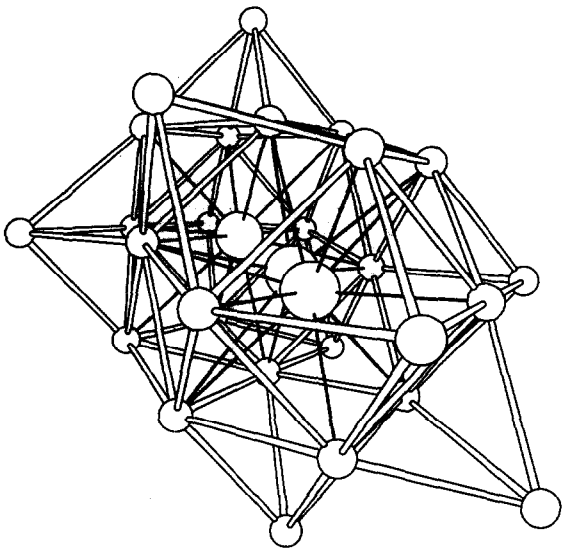

Fig. 11. A gateway minimum of the saddle point of fig. 10. All argons within 6 Å of a fluorine atom are shown.

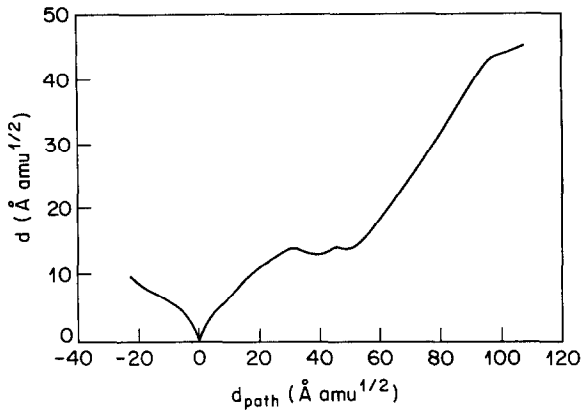

Fig. 12. The reaction path corresponding to figs. 6 and 7. The Cartesian distance of the reaction path configurations from the saddle point configuration is plotted as a function of distance along the reaction path.

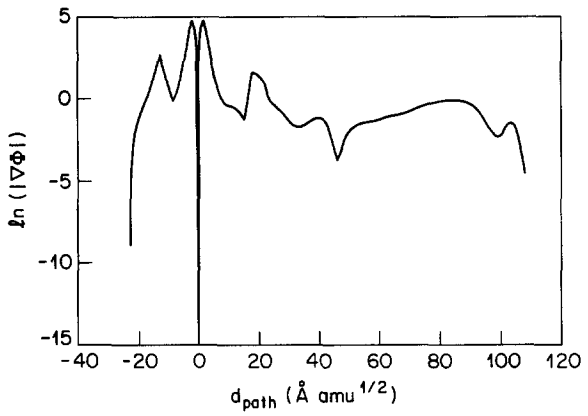

Fig. 14. The reaction path corresponding to figs. 6 and 7. The logarithm of the gradient of the potential energy (mass-weighted coordinates) is plotted as a function of the distance along the reaction path.

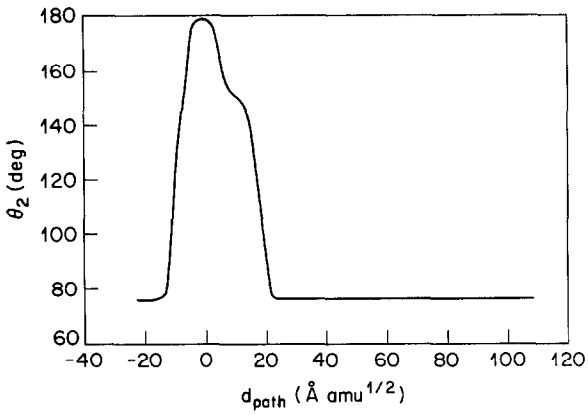

Fig. 13. The reaction path corresponding to figs. 6 and 7. The fluorine bond angle θ_2 is shown as a function of the distance along the reaction path.

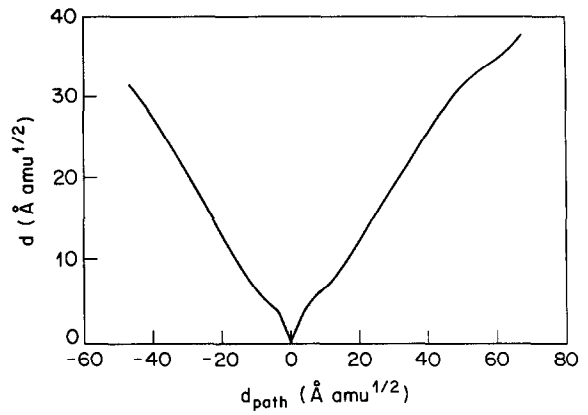

Fig. 15. The reaction path corresponding to figs. 8 and 9. The Cartesian distance of the reaction path configurations from the saddle point configuration has been displayed as a function of distance along the reaction path.

be compared with the fairly direct path followed in the gas phase reaction.

The reaction paths also show two types of descent distinguished by the two types of minima reached. In the first group of minima, the fluorine atoms are almost collinear and θ_2 is between 140° and 160° (fig. 16). In the other group the arrangement of the fluorine atoms resembles the gas phase isosceles triangle minimum and θ_2 is slightly less than 80° (fig. 13). We will refer to these two types of minima as "linear" and "triangular" minima, respectively. The variation of θ_2 in the path to a linear minimum is quite irregular as shown in fig. 16. For the triangular minimum there is a rapid and monotonic change in θ_2 from 140° to 80° after which there are only slight variations in this angle.

The erratic behavior of the gradient shows the existence of "steps" along the reaction path. These presumably lie in the vicinity of nonreactive saddle points that involve rearrangement of solvent atoms.

In contrast with the liquid, the reaction paths in the solid are much shorter and more direct as illus-

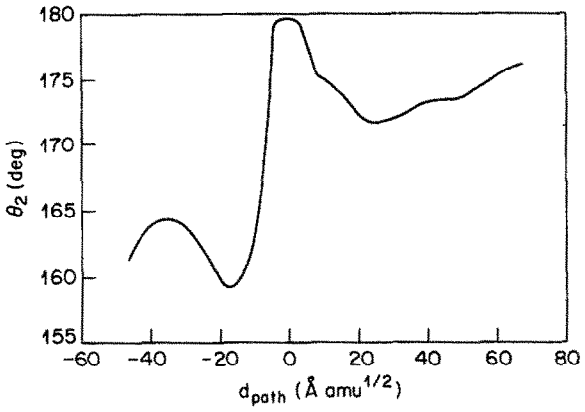

Fig. 16. The reaction path corresponding to figs. 8 and 9. The fluorine bond angle θ_2 appears as a function of the distance along the reaction path.

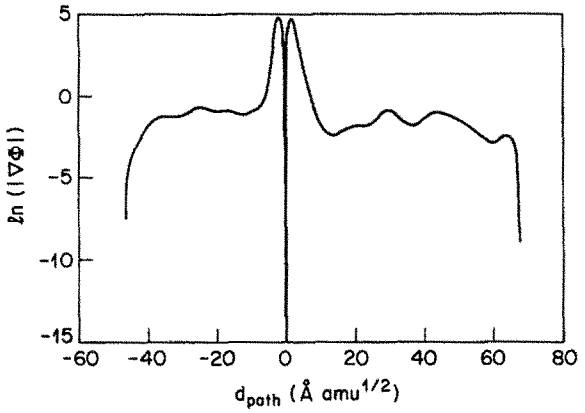

Fig. 17. The reaction path corresponding to figs. 8 and 9. The logarithm of the gradient of the potential energy (mass-weighted coordinates) is shown as a function of the distance along the reaction path.

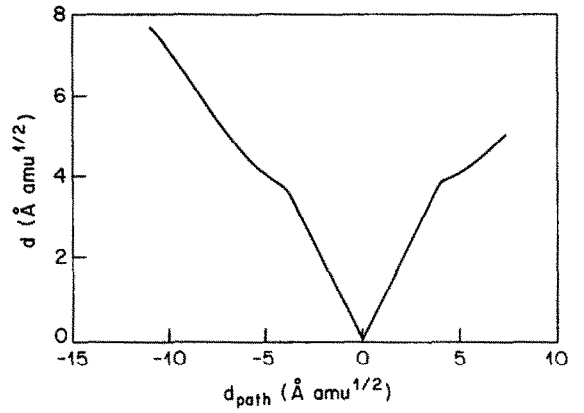

Fig. 18. The reaction path corresponding to figs. 10 and 11. The Cartesian distance of the reaction path configurations from the saddle point configuration is exhibited as a function of distance along the reaction path.

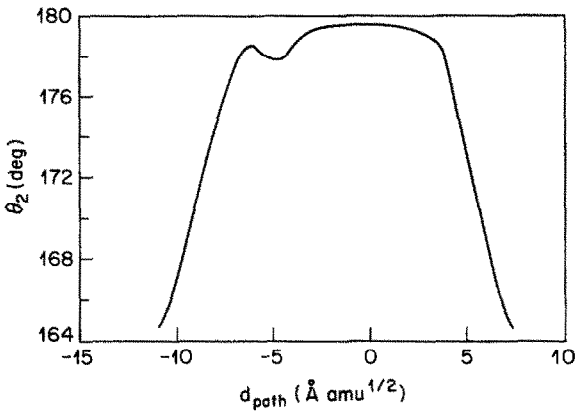

Fig. 19. The reaction path corresponding to figs. 10 and 11. The fluorine bond angle θ_2 is plotted as a function of the distance along the reaction path.

trated in figs. 18–20. This is due to the constraints on the solvent atoms imposed by the lattice. The motion of the fluorine atoms accounts for almost all of the displacement along the reaction path. An interesting feature of this reaction path is that in spite of its asymmetry, the energies of both gateway minima are identical to within the accuracy of the calculation. This study carried out on a saddle point from a solid configuration after the annealing produced similar results, but the gateway minima energies were split by 0.06 kJ/mol.

In this case the solvation has a weak, but measurable effect on the transition states of the reaction. These effects are illustrated by the distribution of properties of the transition states shown in figs. 24–27. Fig. 24 shows shows a histogram of the negative eigenvalues along the reaction coordinate of all of the saddle points located in the 125 argon system. The distribution shows that on average, the fluorine–argon interactions depress the magnitude of this eigenvalue – they broaden the potential barrier. Figs. 25 and 26 illustrate the geometric properties of the saddle points

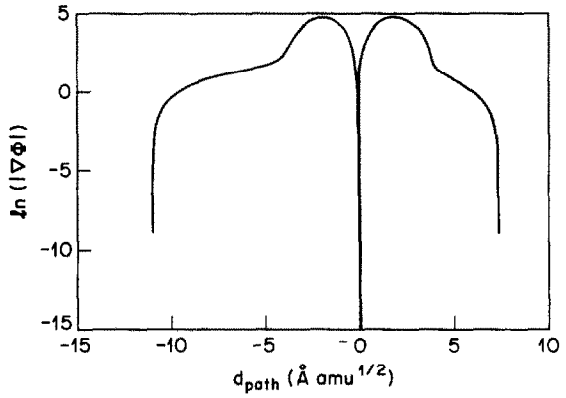

Fig. 20. The reaction path corresponding to figs. 10 and 11. The logarithm of the gradient of the potential energy (mass-weighted coordinates) is provided as a function of the distance along the reaction path.

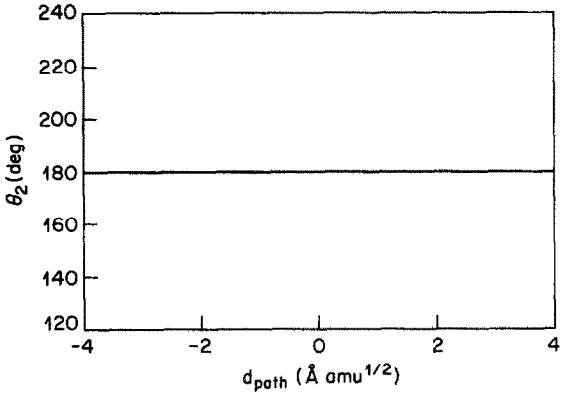

Fig. 22. The reaction path of isolated fluorine. The fluorine bond angle θ_2 is shown as a function of the distance along the reaction path.

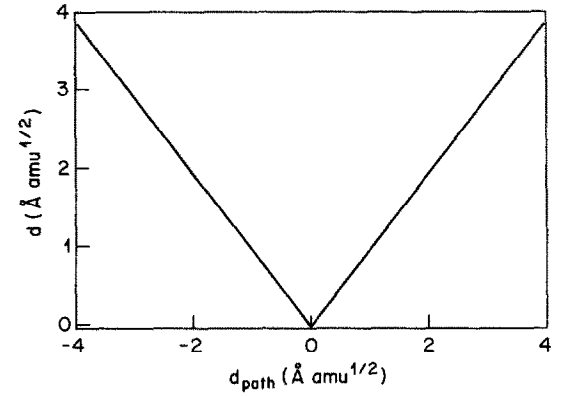

Fig. 21. The reaction path of isolated fluorine. The Cartesian distance of the reaction path configurations from the saddle point configuration is graphed as a function of distance along the reaction path.

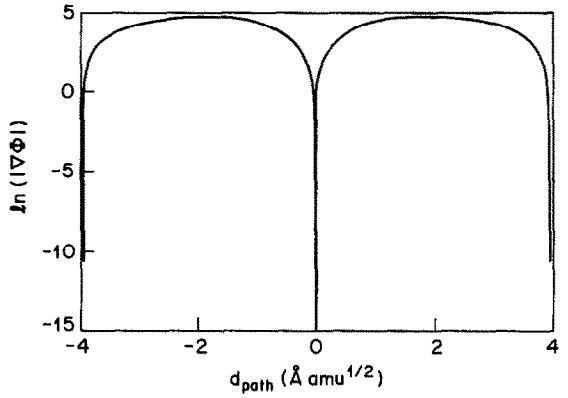

Fig. 23. The reaction path of isolated fluorine. The logarithm of the gradient of the potential energy (mass-weighted coordinates) appears as a function of the distance along the reaction path.

found. The angular distribution shows that the transition complexes are all very close to linear. The distribution of asymmetric stretch values is unimodal around zero. The largest shifts in the asymmetric stretch are about 0.04 of the F_2 bond length.

The distribution of energy differences between the saddle points and their neighboring gateway minima is bimodal, as revealed in the histogram of fig. 27. Further examination shows that this bimodality is due to the existence of both the triangular and linear gateway minima, unlike the gas phase for which only the linear gateway minima exist. This point is illustrated in the scatter plot of θ_2 versus the energy difference, fig. 28. The energy difference for the linear and triangular minima tend to cluster around their respective gas phase values, although there is a significant variation in them. The points with very large energy differences occasionally may be artifacts of the minimization algorithm (MINOP reaching the wrong minimum); however, the full steepest descent calculations illustrated in figs. 12–17 show that reaction paths to both group of minima exist.

The significant differences between the structure of the gateway minima in the gas phase and in solution

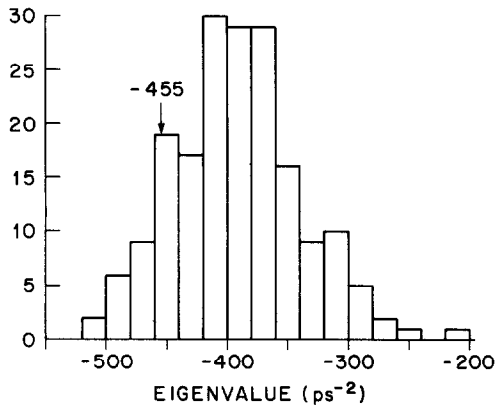

Fig. 24. Histogram of the reaction coordinate eigenvalues of the reactive saddle points for the $\rho_{Ar} = 1.42$ g/ml system. The arrow denotes the eigenvalue of the gas phase saddle point (−454.7).

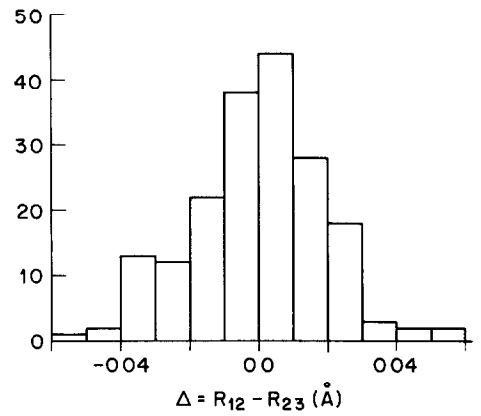

Fig. 25. Histogram of the asymmetric stretches (Å) of the reactive saddle points for the $\rho_{Ar} = 1.42$ g/ml system.

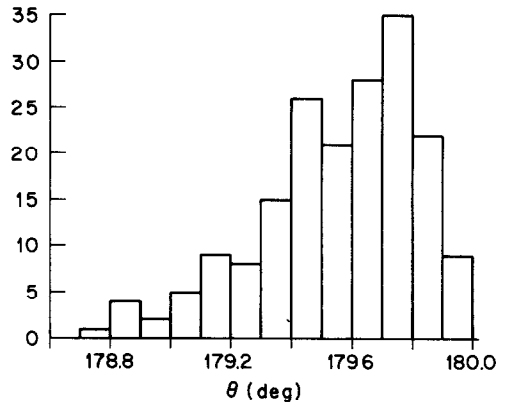

Fig. 26. Histogram of the fluorine bond angles around the central fluorine for the reactive saddle points of the $\rho_{Ar} = 1.42$ g/ml system.

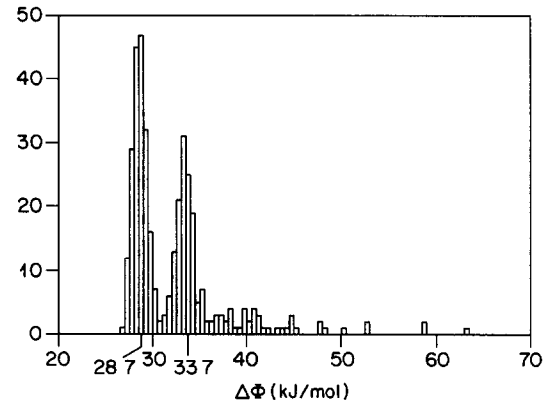

Fig. 27. Histogram of energy differences between saddle points and flanking gateway minima.

can be attributed to the fact that the attraction between the more loosely bound fluorine to the covalently bonded pair is of the same order of magnitude as the argon–argon and argon–fluorine interactions. In contrast, at the saddle point, the magnitude of the eigenmodes involving the stretches and bends of the fluorines are much higher than those involving the argon–fluorine interactions; hence the solvent's effects on the geometry of the transition state are smaller.

We have also looked at whether the structure of one gateway minimum determines the structure of the other. The statistical distribution of the four possible pairings of gateway minima, summarized by table 3, suggests that any such correlations are very weak.

7. Discussion

The example we have studied represents the weak solvation limit. The change in the structure of the fluorine at the transition state induced by the solvent is rather small. Nevertheless, a significant portion of the solvent induced recrossings of the variational transition state dividing surface appear to be due to the shift in the position of the real saddle point – many trajectories which recross the variational transition surface

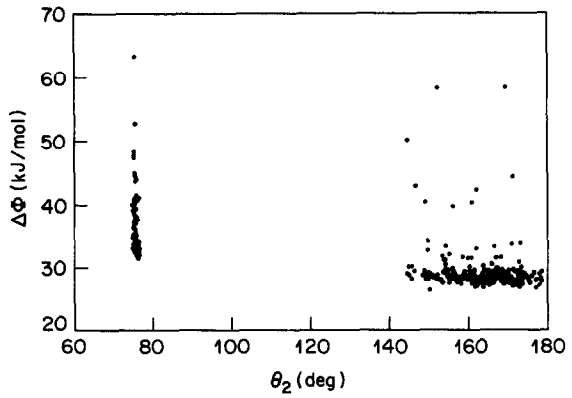

Fig. 28. Scatter plot of the energy differences between the saddle points and gateway minima as a function fo the gateway minimum's bond angle around the central fluorine.

never cross the inherent structure transition surface.

When the solvent effects are much stronger, such as when changes in the charge distribution among the reactants occurs in a strong dielectric solvent (e.g., an S_N2 reaction in water), the change in the reactant geometry at the transition state can be much larger. It is even possible that there could be a bimodal distribution of transition states. For example in the atom–molecule exchange reaction the histogram of the asymmetric stretch can have two or more peaks on either side of the gas phase transition state value. In such strongly solvated cases, even a larger fraction of the recrossings of the variational transition surface may arise from trajectories which never cross a real saddle point.

This effect is similar to that described by the "frozen adiabatic solvent" model of Gertner et al. [38] in which the transition state is shifted by changes in solvation, represented by changes in one hypothetical "solvent variable". Although their theory prescribes a method of calculating the recrossing correction based upon the solvation forces present at the variational transition surface, it does not provide a definition of this "solvent variable" in terms of the particle positions. In contrast, the inherent structure approach explicitly includes all solvent degrees of freedom so that there are no hidden or undefined variables. It may be possible to provide a rigorous definition of such "reduced" solvent variables in terms of the eigenvectors of the Hessian matrix at the saddle points.

We should point out that there can be significant effects not accounted for by the current version of the inherent structure approach. In the gas phase there are many instances where because of a "bottleneck" in the phase space away from a saddle point, the dividing surface defined by the descent mapping to a saddle point is a very poor choice, especially at elevated temperatures [37]. There is no reason to assume such bottlenecks in the phase space do not exist for reactions in solution. In fact, such a bottleneck in the potential energy surface describing a gas phase reaction should imply the existence of one in the presence of a weak solvent. The improvement of the present approach to deal with these bottlenecks in solution would be a major improvement of our theory.

The inherent structure theory provides a systematic approach to exploring the effects of a solvent on a chemical reaction. It requires no assumptions about the reaction coordinate or its coupling to other degrees of freedom. The theory is valid as long as the basins of the reactive saddle points are the bottlenecks of the reaction, although it should be possible to extend the approach beyond this limitation. The

Table 3
Saddle points characterized by geometry of flanking gateway minima. Fraction of saddle points with each characteristic [a]

		(+) Minimum		
		linear	triangular	linear or triangular
(−) Minimum	linear	0.422	0.146	0.568
	triangular	0.184	0.249	0.433
	linear or triangular	0.605	0.395	

[a] I.e. 42.2% of the saddle points found have linear minima on both sides of the saddle point. The (+) and (−) minima of a saddle point are its two flanking minima.

structure and energy of the real saddle points have an important influence on the reaction rate, especially at low temperatures. By analyzing the properties of the saddle points we can understand the mechanism by which a solvent can drastically change a reaction rate. The normal modes and their frequencies at each saddle point can be used to correct the Kramers reaction rate in a way similar to Pollak's demonstration that the exact eigenfrequencies along a reaction coordinate coupled to a one-dimensional harmonic bath can improve the Kramers expression for that simple model [39].

In general, the "solvent" could include many of the degrees of freedom of a complicated reactant molecule. For example, in proteins a seemingly local motion such as the rotation about a bond can be strongly coupled to the motions of atoms far away from the bond, e.g., to move an aromatic ring may require other atoms to first move out of its way via rotations about other bonds [40]. In such cases, there may be multiple reaction paths and reaction coordinates involving many atoms. The development of computational and theoretical approaches to identifying these paths and their relative contributions to the rate constant (i.e. eqs. (2.12) and (2.13)) would enable us to understand the mechanisms of ligand–receptor binding, protein folding, and other important biochemical processes. Such advances would also elucidate factors affecting the rates of conformational changes of molecules in solution (e.g., butane, stilbene, and polymers) and the diffusion of molecules through polymers, zeolites, and biological membranes.

References

[1] H.A. Kramers, Physica 7 (1940) 284.
[2] S. Glasstone, K.J. Laidler and H. Eyring, The Theory of Rate Processes (McGraw-Hill, New York, 1941) ch. 8.
[3] D.G. Truhlar, W.L. Hase and J.T. Hynes, J. Phys. Chem. 87 (1983) 2664
[4] T. Yamamoto, J. Chem. Phys. 33 (1960) 281.
[5] F.H. Stillinger, in: Theoretical Chemistry, Advances and Perspectives, Vol. 3, eds. H. Eyring and D. Henderson (Academic Press, New York, 1978) pp. 209–223.
[6] D. Chandler, J. Chem. Phys. 68 (1978) 2959.
[7] R.W. Zwanzig, Ann. Rev. Phys. Chem. 16 (1965) 67.
[8] F.H. Stillinger, T.A. Weber and R.A. La Violette, J. Chem. Phys. 85 (1986) 6460.
[9] J.P. Bergsma, B.J. Gertner, K.R. Wilson and J.T. Hynes, J. Chem. Phys. 86 (1987) 1356.
[10] R. Alimi, R.B. Gerber and V.A. Apkarian, J. Chem. Phys. 92 (1990) 3551.
[11] F.H. Stillinger and T.A. Weber, Phys. Rev. A 25 (1982) 978.
[12] F.H. Stillinger and T.A. Weber, Phys. Rev. A 28 (1983) 2408.
[13] F.H. Stillinger and R.A. La Violette, J. Chem. Phys. 83 (1985) 6413.
[14] F.H. Stillinger, J. Chem. Phys. 89 (1988) 4180.
[15] L.J. Root and F.H. Stillinger, Phys. Rev. B 41 (1990) 2348.
[16] F.H. Stillinger, Phys. Rev. B 41 (1990) 2409.
[17] F.H. Stillinger, in: Statphys 16, ed. H.E. Stanley (North-Holland, Amsterdam, 1986) pp. 142–149.
[18] F.H. Stillinger and T.A. Weber, J. Chem. Phys. 88 (1988) 5123.
[19] T.A. Weber and F.H. Stillinger, Phys. Rev. B 32 (1985) 5402.
[20] F.H. Stillinger, J. Chem. Phys. 88 (1988) 380.
[21] D.G. Truhlar, A.D. Isaacson and B.C. Garrett, in: Theory of Chemical Reaction Dynamics, Vol. 4, ed. M. Baer (CRC Press, Boca Raton, 1985) p. 65.
[22] J. Chandrasekhar, S.F. Smith and W.L. Jorgensen, J. Am. Chem. Soc. 107 (1985) 154.
[23] G. Herzberg, Molecular Spectra and Molecular Structure, Vol. 1. Spectra of Diatomic Molecules (Van Nostrand–Reinhold, New York, 1950) p. 527.
[24] K.P. Huber and G. Herzberg, Molecular spectra and Molecular Structure, Vol. 4. Constants of Diatomic Molecules (Van Nostrand–Reinhold, New York, 1979) p. 214.
[25] W.F. van Gunsteren and H.J.C. Berendsen, GROMOS Manual, Laboratory of Physical Chemistry, University of Groningen, The Netherlands (1988).
[26] K. Singer, A. Taylor and J.V.L. Singer, Mol. Phys. 33 (1977) 1757.
[27] T.P. Straatsma, H.J.C. Berendsen and J.P.M Postma, J. Chem. Phys. 85 (1986) 6720.
[28] G. Ciccotti, M. Ferrario, J.T. Hynes and R. Kapral, Chem. Phys. 129 (1989) 241.
[29] H.C. Andersen, J. Comput. Phys. 52 (1983) 24.
[30] E. Helfand, J. Chem. Phys. 71 (1979) 5000.
[31] E.A. Carter, G. Ciccotti, J.T. Hynes and R. Kapral, Chem. Phys. Letters 156 (1989) 472.
[32] W.F. van Gunsteren and H.J.C. Berendsen, Mol. Phys. 34 (1977) 1311.
[33] H.J.C. Berendsen, J.P.M. Postma, W.F. van Gunsteren, A. Dinola and J.R. Haak, J. Chem. Phys. 81 (1984) 3684.
[34] R.A. LaViolette and F.H. Stillinger, J. Chem. Phys. 83 (1985) 4079.
[35] J. Baker, J. Comput. Chem. 7 (1986) 385.
[36] L. Kaufman, Computer program MINOP.
[37] P. Pechukas, in: Dynamics of Molecular Collisions, Part B, ed. W.H. Miller (Plenum Press, New York, 1976) p. 269.
[38] B.J. Gertner, J.P. Bergsma, K.R. Wilson, S. Lee and J.T. Hynes, J. Chem. Phys. 86 (1987) 1377.
[39] E. Pollak, J. Chem. Phys. 85 (1986) 865.
[40] J.A. McCammon, Rept. Progr. Phys. 47 (1984) 1.